# Communication—Electrochemical Impedance Signature of a Non-Planar, Interdigitated, Flow-Through, Porous, Carbon-Based Microelectrode

**Zhenglong Li,[1] Yu-Hsuan Cheng,[1,*] Lixin Feng,[2] De Dios Felix,[1] Jacob Neil,[1] Reis Moura Pedro Antonio,[1] Maryom Rahman,[3] Juliana Yang,[2] Samar Azizighannad,[4] Somenath Mitra,[5] and Sagnik Basuray[1,2,z]**

[1]*Department of Chemical and Materials Engineering, New Jersey Institute of Technology, Newark, New Jersey 07102, USA*
[2]*Department of Biomedical Engineering, New Jersey Institute of Technology, Newark, New Jersey 07102, USA*
[3]*Kearny High School, Kearny, New Jersey 07032, USA*
[4]*Department of Materials Science and Engineering, New Jersey Institute of Technology, Newark, New Jersey 07102, USA*
[5]*Department of Chemistry and Environmental Science, New Jersey Institute of Technology, Newark, New Jersey 07102, USA*

Top and bottom microelectrode glass slide sandwiches a channel made of adhesive tape and packed with reduced graphene oxide to make a new non-planar interdigitated microfluidic device. Novel device integration allows packing of any transducer material at room temperature with no instrument. Electrical impedance spectroscopy signal is stable over long times, fits an equivalent circuit with well-defined circuit elements. Flow visualization concurs that electric double-layer signal shifts to high frequency due to disruption of the diffusive process from increased convective flow. Charge transfer resistance appears at higher frequencies making the device rapid with high signal to noise ratio.

 [DOI: 10.1149/2.0041916jes]

Manuscript submitted August 28, 2019; revised manuscript received October 29, 2019. Published November 22, 2019.

Electrical impedance spectroscopy (EIS) using carbon-based (like carbon nanotubes (CNT), graphene oxide (GO)) nano-ordered electrodes, has emerged as a promising electrochemical measurement method for rapid, economical, highly selective, and label-free detection of a diverse range of analytes.[1–9] The carbon-based nanomaterials have extraordinary electron transport, wide electrochemical window, excellent physical properties, superb biocompatibility, and shares the π electron cloud with attached biomolecules to significantly increases the conductance.[10–12] Micro-electrodes (μEs) have been widely applied in EIS due to low ohmic potential drop, the fast establishment of steady-state signal, and increased signal-to-noise ratio (SNR).[7,8,13–16]

In planar interdigitated microelectrode (P-μIDE), the electric field is limited to the electrode surface and hence cannot capture all the target molecules that are in the channel. The sensitivity of P-μIDE is enhanced by extending the capture molecule using a carbon spacer/carbon nanostructures fabricated by complex and expensive methods, complicated operating protocols, extensive soft-lithography.[7,17–21] Further, the electrical double layer (EDL) (a parasitic capacitor), a measure of the ionic strength only, complicates EIS measurements. Hence, EIS sensors typically operate at a low-frequency range where the EDL capacitor signal is negligible. Low-frequency measurements are associated with increased noise, low SNR, and inherently slow. It is hence imperative that the EDL capacitance shifts to a higher frequency for rapid and sensitive EIS measurements.

Here, a new non-planar interdigitated microelectrode (NP-μIDE) based EIS sensor is shown. The NP-μIDE consists of a microfluidic channel (made with adhesive tape) packed with transducer material (here reduced GO (r-GO)) sandwiched by a top and bottom μE. A new "open process" fabrication, introduced here, allows for the packing of any transducer material. Flow visualization experiments show that the disruption in the diffusion kinetics migrates the EDL to high frequency. In NP-μIDE, the EDL shifts to MHz frequency, which allows the charge transfer resistance to be measured at around 100 kHz, significantly improving device sensitivity and signal to noise ratio (SNR). NP-μIDE is a new shear-enhanced, with highly stable and reliable EIS spectra, continuous flow, flow-through porous electrode, microfluidic sensor. Here, the equivalent circuit model that fits the EIS spectra of the NP-μIDE is discussed in detail.

## Experimental

***Preparation of the NP-μIDE parts.***—The detailed protocol for the synthesis of the reduced r-GO is shown elsewhere.[22] Gold μEs are prepared according to Figure 1a.[23,24] Scanning electron microscope (SEM, JSM-7900F JE01) is used to characterize the microelectrode (Figure 1d). See supplementary for details.

***Packing of non-planar interdigitated microelectrode.***—The detailed packing process is shown in Figure 2. First, two holes for fluid inlet and outlet are drilled into the top μE glass slide using a driller (Central Machinery) with a 1mm-diameter drill bit. Before packing, the μE glass slides (both top and bottom) are cleaned thoroughly by acetone and isopropyl alcohol (The volume ratio of these two solutions is 1:1) in a sonication bath for 15 min at room temperature. Post sonication, μE glass slides are blown dry by an air gun. ARcare 90880 polypropylene double-sided adhesive tape is used as the middle adhesive layer, which is also the fluid channel layer (Figure 2b). The wide operating temperature range (−40°C to 120°C), fast bonding, as well as the excellent biological compatibility makes it a natural choice for the channel layer. A Cricut machine is used to cut the desired channel with 50 mm length, 500 μm width, and 150 μm height (tape height). Post cutting, one side of the tape is peeled away, and the channel is affixed to the bottom μE glass slide (Figure 2c). Around 25mg/ml r-GO suspension solution is prepared using the DI-water before the packing process. A certain amount (∼5ml) of this r-GO suspension solution is located on the Au microelectrode to fill up the channel (Figure 2d). After loading, until the solution evaporates, the top release film of the tape layer is peeled away (Figure 2e). This also removes any r-GO that is not in the channel. Finally, the top μE glass slide is affixed to the channel to get an NP-μIDE device, and the tin-coated copper wire is weld to the gold pads (Figures 2f and 2g). An optical microscope

*Electrochemical Society Student Member.
[z]E-mail: sbasuray@njit.edu

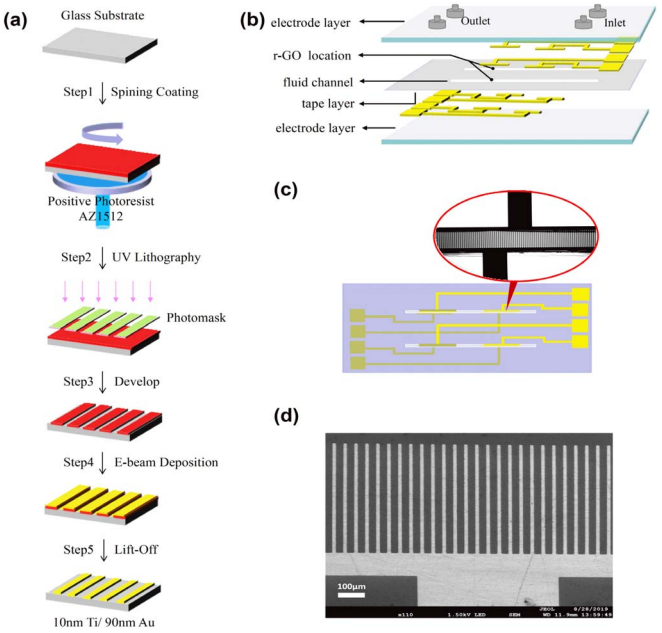


**Figure 1.** (a) Schematic diagram of gold μE fabrication. (b) NP-μIDE sensor. (c) Top view of NP-μIDE chip with interdigitating μE shown in inset. (d) Scanning electron microscope of μE (scale bar is 100μm).

(Olympus BX51) is used to get a perfect overlap between the top and bottom μE glass slides.

***Electrochemical measurements and device run.***—The NP-μIDE is connected to the Impedance analyzer, Agilent 4294A, for EIS readings using standard electrical connections (Figure 2i). EIS readings are taken at 2, 4, 6, and 8-hour intervals for each KCl concentration. Three different chips are used to run the three different KCl concentrations. The NE-300 syringe pump from New Era Pump Systems, Inc. (USA) is used to pass the KCl solution at a flow rate of 1 μl/min.

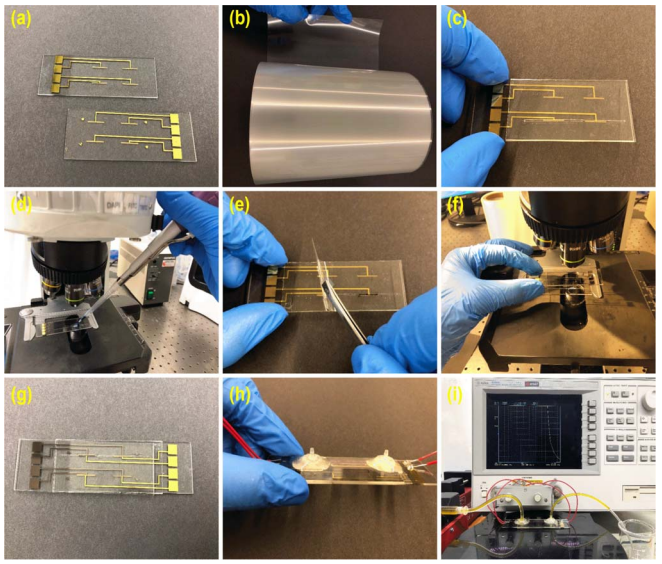


**Figure 2.** (a) – (f) Packing protocol of NP-μIDE. (g, h) r-GO NP-μIDE device. (i) Running of the r-GO NP-μIDE device.

## Results and Discussion

Top and bottom glass slides with an array of gold μEs with dimensions of 500μm × 10μm × 100nm (length × width × height) are used to fabricate the NP-μIDE (Figure 1).[13,25] It is worthwhile to note that the fabrication of the device is tremendously simplified by using an adhesive tape layer to form the microfluidic channel between the gold μEs, as shown in Figure 1a. As opposed to the traditional "closed" preparation method, the use of the tape layer makes the fabrication process of the NP-μIDE device an "open process" (Figure 2). This open process allows the NP-μIDE device to pack any transducer material (CNT, GO, $TiO_2$, among others) between the electrodes. Device integration is carried out at room temperature with no equipment and minimal operator involvement/expertise.

Tightly packaged carbon-based materials have been shown to form 2D and 3D porous structures.[26–30] These carbon-based porous structures increase the contact area between the electrolyte and electrode, leading to enhanced SNR.[7] It is worthwhile to note that our "open design" method allows us to pack the chip with any carbon-based transducer material. Further, these materials can be chemically/physically grafted with any bio-receptor/molecule receptor for use as an EIS sensor. However, to use NP-μIDE as an EIS biosensor, the EIS signal must be consistent across chips. Further, the EIS signature needs to be modeled against an equivalent circuit to obtain relevant sensor data.

Three r-GO packed devices are fabricated to gain a fundamental understanding of NP-μIDE. The EIS spectra (Nyquist Curve) of these three chips for three different concentrations ($1.0 \times 10^{-2}$M, $1.0 \times 10^{-3}$M, $1.0 \times 10^{-4}$M) of KCl solution at different times are shown in Figure 3. These EIS spectra are fitted to the equivalent circuit model in Figure 3a using ZSimpWin software. Both the fitted and experimental data for $1.0 \times 10^{-3}$M KCl solution at the 2-hour mark is shown in Figure 3b ($1.0 \times 10^{-2}$M and $1.0 \times 10^{-4}$M fits at 2 hours are in the supplementary). The circuit elements of the equivalent circuit used to fit the different KCl concentrations are tabulated in Table I. Based on the circuit element values in Table I and the NP-μIDE device, the possible origins of each circuit element can be determined

In the equivalent circuit shown in Figure 3a, Rs represents the resistance from the external circuit. Cc is the cell capacitance that originates from the NP-μIDE electrochemical cell. Here, Rc is the inherent resistance of the device and the r-GO, that is packed in NP-μIDE. The charge transfer resistance (Rct) is associated with the transfer of the charges from the ions in the electrolyte to the tightly-packed r-GO. We assume that the r-GO coverage is extensive enough that none of the ions in the electrolyte interact with the top and bottom gold μEs. This is further collaborated by the EIS signal that shows no characteristic electrode EIS signature. Instead of the ideal double-layer capacitance Cdl, for NP-μIDE, the constant phase element Q due to the inhomogeneity of the interface between the r-GO electrode and electrolyte.[31,32] The highly porous r-GO NP-μIDE electrode should be modeled as an RC transmission line network, which yields the Warburg impedance for highly porous electrodes.[33–35]

Table I gives the detailed parameters of each component in the equivalent circuit at different concentrations. It is worthwhile to note that the low chi-squared value shows that the simulation results fit the experiments very well. The similarity in values of Rc, Rs, and Cc across the three different KCl concentrations confirms our equivalent circuit. Rc, Rs, and Cc values should not change as these components depend on the physical characteristics of the chip itself, as is confirmed by the negligible variation across the three chips in Table I. The decrease of solution ionic strength should increase the EDL length and a concomitant decrease in the value of Q, as is observed here.[23,36,37] Non-idealness of the Cdl capacitor is verified by the deviation of n from 1. As both the Warburg coefficients and Cc does not change, it indicates that for similar packing and packing material, the equivalent circuit/EIS spectra will not change.

Typically, Rct is measured in EIS-based sensors as a change in Rct reflects the binding of target biomolecule on the electrode surface.[38] Figure 3f shows the change in Rct with different KCl concentrations. With the decrease in concentration, we observe a concomitant increase

**Table I. Value of circuit elements in the equivalent circuit under different KCl concentrations.**

| KCl [M] | Rs [ohm] | Cc [F] | Rc [ohm] | Q [S-sec$^n$] | n | Rct [ohm] | W [S-sec$^{0.5}$] | Chi Square |
|---|---|---|---|---|---|---|---|---|
| $1.0 \times 10^{-2}$ | 60.8 | $1.23 \times 10^{-10}$ | 190.2 | $1.6 \times 10^{-7}$ | 0.8832 | 96.4 | $2.94 \times 10^{-18}$ | $2.05 \times 10^{-3}$ |
| $1.0 \times 10^{-3}$ | 26.6 | $3.02 \times 10^{-11}$ | 146.4 | $1.24 \times 10^{-7}$ | 0.8492 | 882.5 | $2.39 \times 10^{-18}$ | $7.22 \times 10^{-3}$ |
| $1.0 \times 10^{-4}$ | 40 | $3.2 \times 10^{-11}$ | 140.7 | $4.38 \times 10^{-8}$ | 0.7542 | 1781 | $2.4 \times 10^{-18}$ | $1.74 \times 10^{-2}$ |

in Rct (Table I) in the EIS spectra. We can see from Figure 3g that Rct does not change with time, which shows excellent stability. From these results, we can confirm that the tightly packaged r-GO is intact even under the flow of 1 μl/min of the KCl solution (translates to about 1mm/s for an empty NP-μIDE chip). Hence, it can be suitably concluded that the equivalent circuit in Figure 3a readily fits the experimental data from the NP-μIDE device. These observations provide adequate theoretical support for the future application of this NP-μIDE chip as a biosensor.

Rct is dominated by the EDL capacitor signal in EIS spectra. Hence, Rct can be measured from the EIS signal only at low frequency.[38] However, EIS signals in the low-frequency region are affected by the noise from external sources leading to poor SNR.[39–41] Hence, low-frequency measurements take a long time to obtain an EIS signal with high SNR.[42,43] Thus, there is a need to shift the Rct to high frequency. This is accomplished in our NP-μIDE device by employing a flow-based detection mode. EDL is the charge stored at the interface between electrode and electrolyte due to diffusion dynamics.[44] The Nyquist plots (Figure 3) indicate that the EDL capacitor discharges at a significantly higher frequency (∼300 kHz) in comparison to other EIS spectra found in the literature (1Hz to 1kHZ) which shifts the Rct to significantly higher frequency.[45–47] This shift is due to the disruption in the diffuse layer dynamics through the introduction of enhanced convective transport from the packed r-GO. It is worthwhile to note that the EIS data from 1 kHz to 100 MHz takes a mere 30 seconds to obtain even after 8 points averaging method used by us for noise reduction.

Flow visualization experiments are used to verify this conjecture. Two proof-of-principle chips are made, as shown in Figures 4a–4d to prove this assumption. Commercially available, blue, yellow, and orange water-soluble food dyes from Modern Biology Inc. flow through the NP-μIDE device at a flow rate of 1μl/min. In the non-packed channel (Figures 4a, 4c), no mixing is seen. However, Figures 4b, 4d shows a well-mixed stream right at the end of the tightly-packed zone of the channel. This demonstrates that intense convective fluxes (increased mixing) are introduced into the microchannel due to the packing. Hence the shift in the EIS signal (Figure 4) to high frequency results from the disruption of the EDL diffusion dynamics due to the increase in the convective transport from the packing of the r-GO.

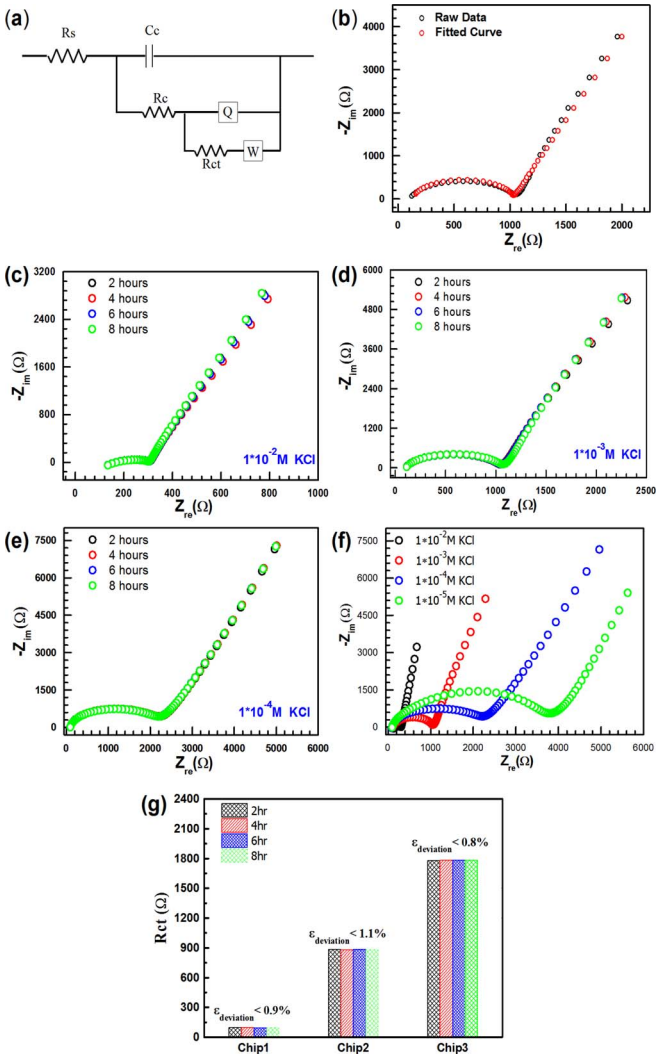


**Figure 3.** (a) Equivalent circuit diagram. (b) Black and Red curves are the Nyquist plot and the fitted curve using 3(a) of the EIS response in $1.0 \times 10^{-3}$M KCl. Nyquist plot of (c) Chip 1, (d) Chip 2, and (e) Chip 3 are at $1.0 \times 10^{-2}$M, $1.0 \times 10^{-3}$M, $1.0 \times 10^{-4}$M KCl concentrations, respectively at 2, 4, 6 and 8 hours. (f) Nyquist plot for different KCl concentrations at 2 hours. (g) Rct of all chips at all times.

## Summary

This study gives a detailed description of a new non-planar interdigitated microelectrode sensor. We have demonstrated a new open process of fabricating the device that allows for any transducer material to be loaded in the device at room temperature with no equipment and with minimal operator expertise/involvement. The device is stable over long times, as is confirmed by the Nyquist curve. An equivalent RC circuit shows good agreement with the experimental

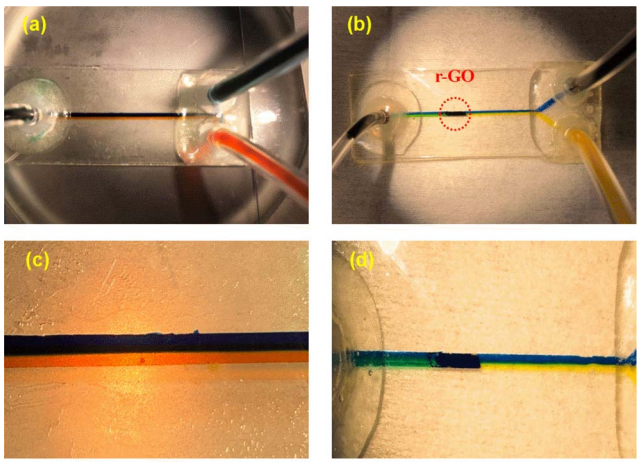


**Figure 4.** Flow-profile of food dyes at 1 μl/min is shown in (a) empty channel and from an r-GO packed channel in (b). (c), (d) are enlarged images of (a), (b) respectively.

results. Flow visualization experiments confirm that the enhanced convective transport due to the packing disrupts the diffusional dynamics, shifting the EDL capacitor to high frequencies. Thus, the charge transfer resistance is seen at significantly high frequency resulting in a rapid, shear-enhanced, continuous flow, flow-through porous electrode. These qualities should make the NP-μIDE microfluidic device a highly sensitive and selective biosensor.

## Acknowledgment

This material is supported by NSF grant # 1751795 "CAREER: "ASSURED" electrochemical platform for multiplexed detection of Cancer Biomarker Panel using Shear-Enhanced Nanoporous-Capacitive Electrodes" to PI Sagnik Basuray.

## ORCID

Zhenglong Li https://orcid.org/0000-0001-9139-7004
Yu-Hsuan Cheng https://orcid.org/0000-0003-2660-6425
Sagnik Basuray https://orcid.org/0000-0001-9767-9096

## References

1. P. Sekhar, Z. Moore, S. Aravamudhan, and A. Khosla, *Sensors*, **17**, 2759 (2017).
2. A. Manickam, C. A. Johnson, S. Kavusi, and A. Hassibi, *Sensors*, **12**, 14467 (2012).
3. M. L. Yola and N. Atar, *Journal of The Electrochemical Society*, **164**, B223 (2017).
4. L. Bai, R. Yuan, Y. Chai, Y. Zhuo, Y. Yuan, and Y. Wang, *Biomaterials*, **33**, 1090 (2012).
5. L. Dai, W. Meng, W. Meng, H. Zhou, G. Yang, Y. Li, and L. Wang, *Journal of The Electrochemical Society*, **163**, B1 (2016).
6. K. Jüttner, *Electrochimica Acta*, **35**, 1501 (1990).
7. H. Sugime, T. Ushiyama, K. Nishimura, Y. Ohno, and S. Noda, *Analyst*, **143**, 3635 (2018).
8. A. Forner-Cuenca, E. E. Penn, A. M. Oliveira, and F. R. Brushett, *Journal of The Electrochemical Society*, **166**, A2230 (2019).
9. S. Kassegne, M. Vomero, R. Gavuglio, M. Hirabayashi, E. Özyilmaz, S. Nguyen, J. Rodriguez, E. Özyilmaz, P. van Niekerk, and A. Khosla, *Microelectronic Engineering*, **133**, 36 (2015).
10. R. H. Baughman, A. A. Zakhidov, and W. A. De Heer, *Science*, **297**, 787 (2002).
11. K. Balasubramanian and M. Burghard, *Analytical and Bioanalytical Chemistry*, **385**, 452 (2006).
12. Z. Zhang, J. Zhang, G. Kwong, J. Li, Z. Fan, X. Deng, and G. Tang, *Sci Rep*, **3**, 2575 (2013).
13. J. Min and A. J. Baeumner, *Electroanalysis: An International Journal Devoted to Fundamental and Practical Aspects of Electroanalysis*, **16**, 724 (2004).
14. D. Li, C. Wang, G. Sun, S. Senapati, and H. C. Chang, *Biosens Bioelectron*, **97**, 143 (2017).
15. A. Parthasarathy, B. Dave, S. Srinivasan, A. J. Appleby, and C. R. Martin, *Journal of The Electrochemical Society*, **139**, 1634 (1992).
16. A. Bezegh and J. Janata, *Journal of The Electrochemical Society*, **133**, 2087 (1986).
17. A. S. Ghrera, C. M. Pandey, and B. D. Malhotra, *Sensors and Actuators B: Chemical*, **266**, 329 (2018).
18. J. Li, H. T. Ng, A. Cassell, W. Fan, H. Chen, Q. Ye, J. Koehne, J. Han, and M. Meyyappan, *Nano Letters*, **3**, 597 (2003).
19. E. Kostal, S. Kasemann, C. Dincer, and S. Partel, *Proceedings*, **2**, 899 (2018).
20. B. Sarada, T. N. Rao, D. Tryk, and A. Fujishima, *Journal of the Electrochemical Society*, **146**, 1469 (1999).
21. A. Khosla and B. Gray, in *Electroactive Polymer Actuators and Devices (EAPAD)* 2010, p. 76421V (2010).
22. S. Azizighannad and S. Mitra, *Sci. Rep.*, **8**, 10083 (2018).
23. S. Basuray, S. Senapati, A. Aijian, A. R. Mahon, and H. C. Chang, *ACS Nano*, **3**, 1823 (2009).
24. S. Senapati, S. Basuray, Z. Slouka, L. J. Cheng, and H. C. Chang, *Topics in Current Chemistry*, **304**, 153 (2011).
25. K. V. Singh, A. M. Whited, Y. Ragineni, T. W. Barrett, J. King, and R. Solanki, *Analytical and Bioanalytical Chemistry*, **397**, 1493 (2010).
26. J. H. Knox, B. Kaur, and G. R. Millward, *Journal of Chromatography A*, **352**, 3 (1986).
27. L. L. Zhang, R. Zhou, and X. Zhao, *Journal of Materials Chemistry*, **20**, 5983 (2010).
28. Y. Zhu, S. Murali, M. D. Stoller, K. Ganesh, W. Cai, P. J. Ferreira, A. Pirkle, R. M. Wallace, K. A. Cychosz, and M. Thommes, *Science*, **332**, 1537 (2011).
29. W. Li, R. Fang, Y. Xia, W. Zhang, X. Wang, X. Xia, and J. Tu, *Batteries & Supercaps*, **2**, 9 (2019).
30. J. Lee, J. Kim, and T. Hyeon, *Advanced Materials*, **18**, 2073 (2006).
31. J. Dygas, B. Misztal-Faraj, Z. Florjańczyk, F. Krok, M. Marzantowicz, and E. Zygadło-Monikowska, *Solid State Ionics*, **157**, 249 (2003).
32. J. Fleig, P. Pham, P. Sztulzaft, and J. Maier, *Solid State Ionics*, **113**, 739 (1998).
33. J. Nielsen, T. Jacobsen, and M. Wandel, *Electrochimica Acta*, **56**, 7963 (2011).
34. J. Wang and J. Bates, *Solid State Ionics*, **18**, 224 (1986).
35. B. A. Boukamp and H. J. Bouwmeester, *Solid State Ionics*, **157**, 29 (2003).
36. S. Basuray and H. C. Chang, *Physical Review. E, Statistical, Nonlinear, and Soft Matter Physics*, **75**, 060501 (2007).
37. S. Basuray and H. C. Chang, *Biomicrofluidics*, **4**, 13205 (2010).
38. S. Basuray, S. Senapati, A. Aijian, A. R. Mahon, and H.-C. Chang, *ACS Nano*, **3**, 1823 (2009).
39. Y. Tan, S. Bailey, and B. Kinsella, *Corrosion Science*, **38**, 1681 (1996).
40. Q. Le Thu, G. Bierwagen, and S. Touzain, *Progress in Organic Coatings*, **42**, 179 (2001).
41. M. Attarchi, M. S. Roshan, S. Norouzi, S. Sadrnezhaad, and A. Jafari, *Journal of Electroanalytical Chemistry*, **633**, 240 (2009).
42. G. Popkirov, *Electrochimica Acta*, **41**, 1023 (1996).
43. R. Alvarez and M. Sanchez, Frequency domain transform and the coulostatic technique, in, De Gruyter, (2002).
44. N. Mavrogiannis, X. Fu, M. Desmond, R. McLarnon, and Z. R. Gagnon, *Sensors and Actuators B: Chemical*, **239**, 218 (2017).
45. N. Tandon, A. Marsano, R. Maidhof, K. Numata, C. Montouri-Sorrentino, C. Cannizzaro, J. Voldman, and G. Vunjak-Novakovic, *Lab on a Chip*, **10**, 692 (2010).
46. G. Justin, M. Nasir, and F. S. Ligler, *Analytical and Bioanalytical Chemistry*, **400**, 1347 (2011).
47. Y. Wang, Z. Ye, J. Ping, S. Jing, and Y. Ying, *Biosensors and Bioelectronics*, **59**, 106 (2014).